






Coriolis massflow measurement errors due to inhomogeneous entrained particles: An analytical model

Stephan Wernli^{a,b} ^{*}, Lilach Goren Huber^c, Nicolas P. Avdelidis^{d,a} , Alfred Rieder^e 

^a Faculty of Engineering and Applied Sciences, Cranfield University, United Kingdom

^b Endress+Hauser Flowtec AG, Switzerland

^c School of Engineering, Zurich University of Applied Sciences, Switzerland

^d Department of Aeronautics and Astronautics, School of Engineering, University of Southampton, United Kingdom

^e Endress+Hauser Flow Deutschland AG, Germany

ARTICLE INFO

Keywords:

Coriolis mass flow meter (CMF)
Multi-phase flow
Flow measurement errors
Bubble theory
Compressibility
Modal modeling

ABSTRACT

The Coriolis mass flow meter is a critical instrument used in various industries for the precise measurement of mass flow rate and density of a fluid. Despite its widespread use, the impact of entrained particles within the fluid can significantly affect the accuracy of the meter, leading to potential errors and inefficiencies. Previous calculations of the mass flow errors assumed that the entrained particles are uniformly distributed along the axis of the measurement tube. In this paper we extend the analytical investigation of the measurement errors beyond the previous work to the regime of non-uniform density distribution of the entrained particles. We provide a clear analysis of the contributions of various physical effects in this regime to the mass-flow measurement error.

1. Introduction

The Coriolis Mass Flow-meter (CMF), known for its broad use in different industrial settings and applications, has the ability to concurrently measure the density and mass flow of a medium [1]. The density measurement is determined by the resonance frequency measured in the tube. The mass-flow measurement is based on the Coriolis principle, which involves a phase shift between two sensors along the tube. Fig. 1 provides a schematic description of the basic mechanical design.

The measurements of density and mass flow, are predicated on the assumption of a homogeneous medium [2]. This assumption is however not always valid as Multi-phase flows are not uncommon in industrial applications of Coriolis flow meters. A common example is the oil and gas industry, where solid particles or gas bubbles are often mixed in the fluid. Other examples are gas bubbles entrained in fluids in the food and beverage or the pharmaceutical industry [1]. The measurement of multi-phase flows, particularly those involving entrained particles, both solid and gas, presents a significant challenge for Coriolis mass flow meters. These devices are renowned for their accuracy and reliability in measuring single-phase fluids, but their performance can be compromised in multi-phase flows by two major perturbation effects, referred to as the phase-decoupling (bubble) and compressibility effect as shown analytically in Basse [3], Rieder and Zhu [4] and experimentally by Weinstein [5], Ibryaeva et al. [6].

These types of errors can lead to significant misreadings in mass-flow and density measurement of up to 50% of the real value according to Basse [3], strongly depending on the type and concentration of particles.

Previous research investigated both analytically and experimentally the two types of measurement errors due to entrained particles [3,7–10]. In all past works an underlying assumption was that the entrained particles are of a uniform size and are uniformly distributed along the measurement pipe. This assumption is, however, unrealistic in many applications, due to various effects. One unavoidable reason are differences in the pressure loss between the two pipe ends, leading to an axial dependence of the size and concentration of the entrained particles. Such asymmetry between the inlet and outlet sides inevitably leads to asymmetric contributions to the Coriolis force acting on the fluid, which in turn directly affect the accuracy of the Coriolis-based flow measurement. *Deriving and estimating the measurement error that results from non-uniform entrained particle distribution is the main contribution of this paper.*

The measurement error in the presence of non-uniform entrained particles is derived here by modifying existing error derivations that did not account for non-uniformity, but assumed that the entrained particles are distributed uniformly along the pipe. As in previous research, we divide the measurement errors to their two main underlying

* Corresponding author at: Faculty of Engineering and Applied Sciences, Cranfield University, United Kingdom.

E-mail address: stephan.wernli@cranfield.ac.uk (S. Wernli).

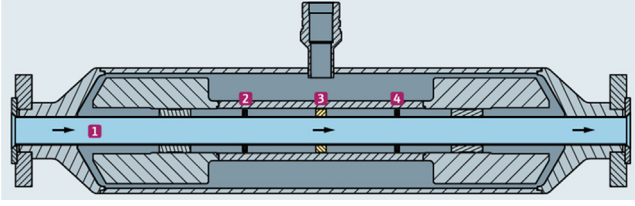


Fig. 1. Coriolis tube model, taken from Endress+Hauser Flow [11]: shows the side-view of a CMF, where number 1 represents the fluid, numbers 2 and 4 depict the first and second sensor units respectively, and number 3 signifies the exciter element.

mechanisms: phase decoupling (or bubble effect) and compressibility (or resonator effect).

Errors due to phase decoupling of the fluid and the entrained particles were derived in Basse [3], Hemp and Kutin [7]. They introduced the phase decoupling model for the mixed fluid, which we use as a starting point and extend in this paper to the non-uniform case.

Measurement errors due to the change in compressibility were derived and investigated in Rieder and Zhu [4], Rieder et al. [8] by introducing the “moving resonator model”. Here we rely on the same modeling approach but extend it to the case of non-uniform entrained particle.

In the following we derive the two model extensions that calculate the measurement errors, including corrections due to non-uniformity. We refer to the previous derivations and specify what modifications are undertaken in order to include effects of non-uniform entrained particles in the existing models. We introduce a simple model of the non-uniformity, quantify individual contributions to these corrections, that stem from different physical mechanisms, and estimate their magnitude based on realistic model parameters in different regimes. To this end, we first introduce the calculation of the measured mass flow for a single-phase fluid, with no entrained particle (Section 2.1). Next we recapitulate on the model of the compressibility related measurement errors [4], extending it for the case of non-uniform flow (Section 2.2.1). Finally, we refer to the model of the phase-decoupling errors [3] and extend it to the non-uniform conditions (Section 2.2.2). The two effects are then combined (Section 2.2.3) in order to calculate the resulting corrections to the measurement errors that were overlooked by previous studies.

2. Mass flow measurement errors due to entrained particles

2.1. Mass flow measurement of a single phase fluid

The Coriolis measurement setup contains a tube through which a fluid is flowing. The tube is connected to an external driver that induces an oscillation of the tube at a certain Frequency. The fluid moving along the oscillating tube experiences a Coriolis force due to the rotation of the reference frame. This force is exerted in opposite directions at the inlet and outlet sides of the tube, thereby exciting an anti-symmetric twist motion in addition to the symmetric transverse bending motion, as illustrated in Fig. 2. The different Coriolis forces at the two ends of the tube create a delay in the oscillation phase of the tube.

By detecting the phase shift caused by the flow, the Coriolis device allows to measure the mass flow of the fluid. The mass flow can be expressed in terms of measurable quantities. This is done by solving the Equation of Motion (EoM) of a fluid of density ρ_f , cross-section area A_f and velocity v_f in a tube of density ρ_t and cross-section area A_t . The EoM describes the transverse motion amplitude x as function of time t and distance z along the tube axis. Due to the flow velocity v_f we introduce the Coriolis term into the standard Bernoulli beam equation (Eq. (1) in Rieder and Zhu [4]):

$$\frac{E_t I_t}{1 - \nu^2} \frac{\partial^4 x}{\partial z^4} + (A_t \rho_t + A_f \rho_f) \frac{\partial^2 x}{\partial t^2} + 2A_f \rho_f v_f \frac{\partial^2 x}{\partial t \partial z} = 0, \quad (1)$$

where E_t , I_t and ν are the elasticity modulus, moment of inertia and Poisson's ratio respectively.

Note that as compared to Rieder and Zhu [4] we divide the elasticity term by the factor $1 - \nu^2$, according to Young and Budynas [12]

As shown in Rieder and Zhu [4], the mass flow \dot{m} of the fluid in the tube is proportional to the time delay Δt between the signals at the inlet and outlet sides of the tube:

$$\dot{m} = c_m \Delta t \quad (2)$$

Using the above relation a measurement of the time delay can be translated to a measurement of the mass flow. The coefficient c_m is shown to obtain the form

$$c_m = \frac{1 - \omega_D^2 / \omega_C^2}{2k_C C_{DC}}. \quad (3)$$

The expressions for ω_D , ω_C , k_C and C_{DC} are obtained by following the lines of Rieder and Zhu [4], which we briefly summarize here. The first step of the calculation is to introduce the dimensionless axial coordinate:

$$\zeta = \frac{2}{l} z, \quad (4)$$

and approximate the solution $x(\zeta, t)$ to the EoM (1) using a linear superposition of the first two Eigenmodes of the beam equation, the symmetric driving mode $a_D(\zeta)$ and the anti-symmetric Coriolis mode $a_C(\zeta)$ (see Fig. 2 for their illustration):

$$a_D(\zeta) = \frac{\cosh \gamma_D \cos(\gamma_D \zeta) - \cos \gamma_D \cosh(\gamma_D \zeta)}{\sqrt{\int_{-1}^1 (\cosh \gamma_D \cos(\gamma_D \zeta) - \cos \gamma_D \cosh(\gamma_D \zeta))^2 d\zeta}} \quad (5)$$

$$a_C(\zeta) = \frac{\sinh \gamma_C \sin(\gamma_C \zeta) - \sin \gamma_C \sinh(\gamma_C \zeta)}{\sqrt{\int_{-1}^1 (\sinh \gamma_C \sin(\gamma_C \zeta) - \sin \gamma_C \sinh(\gamma_C \zeta))^2 d\zeta}} \quad (6)$$

The eigenvalues $\gamma_D = 2.365$ and $\gamma_C = 3.926$ of the well-known Euler–Bernoulli beam equation, which is derived in detail in Chapter 8.5.1 of Singiresu and Nguyen [13], can be calculated by imposing the boundary conditions of a fixed clamped beam:

$$x(\zeta = \pm 1, t) = 0 \quad (7)$$

$$\frac{\partial x}{\partial \zeta}(\zeta = \pm 1, t) = 0. \quad (8)$$

When the tube is excited with an external driving frequency ω_D , the dynamics of the transverse motion is dominated by this frequency and the solution to the EOM can be approximated as:

$$x(\zeta, t) = \text{Re} \left\{ [A_D a_D(\zeta) + A_C a_C(\zeta)] e^{j\omega_D t} \right\} \quad (9)$$

where A_D and A_C are complex amplitudes and the driving frequency ω_D and Coriolis frequency ω_C are given by

$$\omega_{D,C} = \left(\frac{2\gamma_{D,C}}{l} \right)^2 \sqrt{\frac{E_t I_t}{(1 - \nu^2)(A_t \rho_t + A_f \rho_f)}}. \quad (10)$$

The above relations are obtained by multiplying the EoM with each one of the Eigenmodes $a_C(\zeta)$ and $a_D(\zeta)$ (see Rieder and Zhu [4]), and integrating over the tube length. Doing this, and using the relations $\dot{m} = \rho_f v_f$ and $\Delta t = 2\text{Re}[A_C / (j\omega_D A_D)]$ we also obtain Eqs. (2) and (3) with the Coriolis coupling coefficient given by

$$C_{DC} = \int_{-1}^1 a_D'(\zeta) a_C(\zeta) d\zeta, \quad (11)$$

and the yieldingness by

$$k_C = \left(E_t I_t (2\gamma_C / l)^4 \right)^{-1}. \quad (12)$$

Using Eqs. (2)–(12), we can calculate the mass flow of a uniform homogeneous single-phased fluid by measuring the time delay of the oscillation between the two tube ends.

In the next section we discuss the correction to the mass flow when the measured fluid is not homogeneous but rather includes a small fraction of particles that are entrained in the fluid.

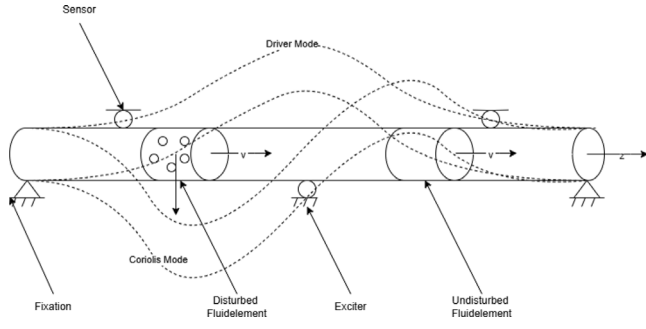


Fig. 2. Schematic description of the first symmetric (driver) and anti-symmetric (Coriolis) mode of the measurement tube: shown are the relevant mechanical components as sensors and exciters as well as the two different kind of fluid elements: homogeneous (single-phase) and mixed (with entrained particles) with a fluid speed v .

2.2. Mass flow corrections due to entrained particles

The mass flow measurement principle in the previous section is based on the assumption that the fluid in the tube is uniform and homogeneous. In operational conditions this assumption does not always hold. The main reason are entrained particles (solid or gas) that are mixed into the host fluid.

Entrained particles influence the mass flow measurement through two main physical effects. Each of these effects leads to potential measurement errors: (1) Errors due to compressibility effects as described in Rieder and Zhu [4] and (2) Errors due to the effect of phase decoupling as mentioned in Basse [3]. Here we extend the discussion by covering regimes of the mixed flow that have not been covered before. In particular, we examine the modifications to both error types caused by potential non-uniformity of the entrained particles along the tube axis.

Note that for the sake of clarity we do not repeat the derivations of the underlying models of Basse [3], Rieder and Zhu [4], but rather sketch their main steps, and elucidate the adaptations needed in order to include the effects of non-uniform entrained particles.

2.2.1. Mass flow corrections due to compressibility effects

The first major source of errors due to entrained particles in the mass flow measurement results from the change in the compressibility of the mixed-phase fluid compared to the uniform single-phase fluid. In this case the coefficient c_m in Eq. (2) above is modified. The change in compressibility is mostly relevant in the case of entrained gas bubbles in a liquid. To understand how c_m is modified we revisit the equation of motion of the Coriolis tube, introducing entrained particles into the fluid. The uniform single-phase Coriolis system is described by the EoM (1) above. The last term on the LHS of (1) is the Coriolis force acting due to the flow velocity v_f being non zero. To derive the measurement error in the presence of entrained gas we follow the lines of the derivation in Rieder and Zhu [4]. In the presence of entrained gas, the model assumes that gas bubbles are uniformly distributed along the pipe and are small relative to the tube diameter, treating the liquid-gas mixture as a homogeneous medium. According to the model all fluid dependent terms can be replaced by an effective force per length $F_{res}(z)$. The effective force can be approximated using a moving resonator model. In this model, due to the added compressibility of the mixed fluid, the tube and fluid are no longer assumed to move together. Instead, the mixture moves with its own effective mass. This additional motion leads to the effective force that can be efficiently expressed in terms of a transfer function $H(j\omega)$:

$$H(j\omega) = (j\omega)^2 A_f \rho_f \left[1 + \frac{r_r}{\frac{\omega_r^2}{\omega^2} + j \frac{\omega_r}{\omega Q_r} - 1} \right] \quad (13)$$

with $r_r = 0.837$ as shown in Rieder and Zhu [4]. Here ω_r and Q_r are the effective resonator frequency and quality factor. The frequency ω_r can be expressed in terms of the modified compressibility, or equivalently the modified speed of sound c_r due to the presence of entrained gas:

$$\omega_r = c_r \frac{1.842}{\pi d} \quad (14)$$

The modified speed of sound in the presence of particles where α represents the gas void fraction (GVF), with a speed of sound c_p in a fluid with a speed of sound c_f and pressure p was derived in Eq. (16) in Rieder and Zhu [4] to be:

$$c_r = \left(\frac{\alpha}{c_p^2} + \frac{(1-\alpha)^2}{c_f^2} + \frac{\alpha(1-\alpha)\rho_f}{\gamma p} \right)^{-\frac{1}{2}} \quad (15)$$

where γ is the adiabatic gas constant. There is no closed solution form for the quality factor Q_r , but it can be determined by experimental tests as described in Rieder and Zhu [4]. In addition to the approach in Basse [14], which accounts for the damping of the tube, fluid and particle decoupling, this factor Q_r also accounts for the attenuation caused by the compressibility of the enclosed particles. The transfer function (13) is a sum of the original force exerted by the tube only, and the additional force due to entrained particles. As a result, the additional force can be viewed as a modification of the effective fluid cross-sectional area on which the force (per length) is exerted:

$$A_f^{comp} = A_f(1 + \Psi) \quad (16)$$

with

$$\Psi = \frac{r_r}{\frac{\omega_r^2}{\omega^2} + j \frac{\omega_r}{\omega Q_r} - 1} \quad (17)$$

As will be shown in Section 2.2.3 below, expressing the entire compressibility effect in terms of a modification to the effective cross sectional area turns out to be useful in order to interpret the origin of measurement errors of the Coriolis device. In this paper we examine yet additional effects of entrained particles, caused by a possible non-uniformity of the properties of the mixed fluid in the axial direction. Such effects are potentially important if they contain an anti-symmetric component that acts differently on the inlet and outlet sides of the tube, thereby changing the Coriolis force and leading to modified measurements. A plausible axial dependence can emerge from pressure differences between the inlet and outlet. This is likely to lead to a non uniform entrained particle distribution along the axis of the tube. We express this effect by letting the Gas Void Fraction (GVF) depend on the axial position as $\alpha = \alpha(\zeta)$. If the ζ dependence of $\alpha(\zeta)$ is not too strong, such that $d\alpha/d\zeta \ll \alpha$, we can use the same resonator model as above and assume that the approximate effect is to introduce a ζ dependence to the quality factor $Q_r = Q_r(\zeta)$ and the speed of sound $c_r = c_r(\zeta)$, and thus to the resonator frequency $\omega_r = \omega_r(\zeta)$, without changing the form of the transfer function. As a result, the effect of non-uniform entrained particles, expressed as a modification of the effective cross-section A_f due to the resonator obtains the form:

$$A_f^{comp}(\zeta) = A_f(1 + \Psi(\zeta)). \quad (18)$$

with

$$\Psi(\zeta) = \frac{r_r}{\frac{\omega_r(\zeta)^2}{\omega^2} + j \frac{\omega_r(\zeta)}{\omega Q_r(\zeta)} - 1} \quad (19)$$

2.2.2. Mass flow corrections due to phase decoupling

A second origin for flow measurement errors in the Coriolis setup is often termed the bubble effect, or decoupling effect. The errors results from the decoupling of transverse motion of entrained particles with density ρ_p from the motion of the surrounding fluid of density ρ_f , due to the difference in mass of the particle and the fluid. The decoupling of the fluid phase from the particle phase leads to a change in the center of mass of the tube and in turn to an apparent mass flow \dot{m}_{dec} which is smaller than the one expected from the uniform fluid, as calculated

by Basse [3] in Eq. (92):

$$\dot{m}_{dec} = \rho_f A_f \left[1 - \alpha Re\{F_{dec}\} \left(\frac{\rho_f - \rho_p}{\rho_f} \right) \right] v_f \quad (20)$$

Similarly to the resonator effect, the mass flow error due to phase decoupling can be expressed in terms of a reduction of the effective cross-sectional area of the fluid A_f on which forces are exerted. In this case the reduction is proportional to the gas volume fraction α , the density difference between the fluid and particle phases and the decoupling force coefficient F_{dec} , which was calculated by Basse and Hemp to obtain the form of Eq. (66) in Basse [3]:

$$F_{dec} = F_{dec}(\omega, \rho_f, \rho_p, \mu_f, \mu_p, a), \quad (21)$$

where μ_f , μ_p are the dynamic viscosities of the fluid and particles respectively, and a is the particle radius. Thus, the modified cross section area due to phase decoupling is

$$A_f^{dec} = A_f(1 + \Phi), \quad (22)$$

with

$$\Phi \equiv -\alpha F_{dec} \left(\frac{\rho_f - \rho_p}{\rho_f} \right). \quad (23)$$

To extend the decoupling model to the regime of non-uniform fluid mixtures, we introduce an axial dependence to the GVF $\alpha = \alpha(\zeta)$, as well as to the effective force coefficient $F_{dec} = F_{dec}(\zeta)$. The ζ dependence of F_{dec} is assumed primarily through the potential dependence of the particle radius on the axial position $a = a(\zeta)$. As a consequence, we adopt a general definition of the correction to the cross sectional area due to decoupling:

$$\Phi(\zeta) = -\alpha(\zeta) F_{dec}(\zeta) \left(\frac{\rho_f - \rho_p}{\rho_f} \right), \quad (24)$$

with the resulting modified axial-dependent cross section:

$$A_f^{dec}(\zeta) = A_f(1 + \Phi(\zeta)). \quad (25)$$

For an in-depth consideration of the effect of α and its components, this can be broken down into a constant part and its symmetric and anti-symmetric residues.

$$\alpha(\zeta) = \alpha_0 + \alpha_{sym}^{res}(\zeta) + \alpha_{asym}^{res}(\zeta) = \alpha_0 + \alpha_4^{res}(\zeta) \quad (26)$$

We note that in this study we account for dependencies along the axial direction of the tube, neglecting any possible dependency of the particle radius and concentration in the radial direction. In each pipe segment along the axis, the model assumptions are identical to those in Table 4 of Basse [3].

2.2.3. Combined effects of entrained particles

Expressing all of the above effects of entrained particles as corrections to the effective area has the advantage that we can now go back to the equation of motion and replace the effective area A_f in front of the fluid density ρ_f , wherever it appears in Eq. (1) by its corrected expression,

$$A_f(\zeta) = A_f(1 + \Psi(\zeta))(1 + \Phi(\zeta)) \simeq A_f(1 + \Psi(\zeta) + \Phi(\zeta)), \quad (27)$$

where in the last step we linearized to first order in the corrections Φ and Ψ . Based on previous findings by Basse [3] that showed that the compressibility correction to the mass term is twice larger than the decoupling correction, we add a factor of 2 in front of $\Psi(\zeta)$ in this term, thus obtaining the corrected EoM,

$$\begin{aligned} & \left(\frac{2}{l} \right)^4 \frac{E_t I_t(\zeta)}{1 - v^2} \frac{\partial^4 x}{\partial \zeta^4} + \\ & + (A_t \rho_t + A_f [1 + \Phi(\zeta) + 2\Psi(\zeta)] \rho_f) \frac{\partial^2 x}{\partial t^2} + \\ & + \frac{2}{l} A_f [1 + \Phi(\zeta) + 2\Psi(\zeta)] \rho_f v \frac{\partial^2 x}{\partial t \partial \zeta} + \\ & - m_v \frac{\partial^2 x}{\partial t^2} = \frac{2}{l} \delta(\zeta) F_E^0. \end{aligned} \quad (28)$$

In this formulation of the EoM we introduced a local drive force F_E^0 at the center of the tube on the RHS, as well as a damping force with a damping coefficient m_v on the LHS. This will allow us a more generic analysis of potential effects on the measurement errors. An additional correction that we allow is due to an axial dependence of the effective moment of inertia $I_t = I_t(\zeta)$. This is potentially the case in the presence of a non-ideal connection between the measuring tube and the coupling elements. Note that in general such an axial dependence could introduce an additional term proportional to $\partial^2 x / \partial \zeta^2$. This term is subdominant if we assume slow enough ζ dependencies.

From the modified equation of motion (28) we now calculate the new relation between the mass flow and time delay. This should lead us to the mass flow measurement error.

To obtain the mass flow, we plug the solution (9) into the modified EoM (28). Next, we multiply both sides of the EoM by $a_C(\zeta)$ and integrate over the entire tube length. Due to symmetry considerations, we are then left with integrals in which the integrands are not purely anti-symmetric over the tube. Now we collect all the terms that are non vanishing after this integration and obtain

$$\begin{aligned} & \underbrace{\left(\frac{2}{l} \right)^4 \frac{E_t I_t}{(1 - v^2)} \gamma_C^4 A_C}_{\text{Stiffness tube}} \\ & + \underbrace{\left(j \left(\frac{2}{l} \right)^4 \frac{E_{tw} I_t}{(1 - v^2)} \gamma_C^4 + j \omega^2 m_v - j \omega^2 \rho_f A_f \Theta_{CC}^{sym,im} \right) A_C}_{\text{Damping tube + fluid + particle}} \\ & - \underbrace{\left(\omega^2 (\rho_t A_t + \rho_f A_f) + \omega^2 \rho_f A_f \Theta_{CC}^{sym,re} \right) A_C}_{\text{Mass tube + fluid + particle}} \\ & = -j \left(\frac{2}{l} \right) 2 \omega \tilde{m} \tilde{C}_{DC} A_D \\ & \quad \underbrace{\hspace{10em}}_{\text{Coriolis fluid} \rightarrow \text{Mass flow}} \\ & \quad - j \left(\frac{2}{l} \right) 2 \omega \tilde{m} \Theta_{DC}^{sym} A_D \\ & \quad \underbrace{\hspace{10em}}_{\text{Coriolis particle} \rightarrow \text{Mass flow shift 1}} \\ & \quad - j \omega^2 \rho_f A_f \Theta_{DC}^{asym} A_D \\ & \quad \underbrace{\hspace{10em}}_{\text{Asym-damping particle} \rightarrow \text{Mass flow shift 2}} \\ & \quad - j \left(\frac{2}{l} \right)^4 \frac{E_{tw} I_{asym}}{(1 - v^2)} \Theta_{DC}^{asym,tube} A_D \\ & \quad \underbrace{\hspace{10em}}_{\text{Asym-damping tube} \rightarrow \text{Mass flow zero}} \end{aligned} \quad (29)$$

Since we are interested in corrections to the mass flow, we kept on the RHS only imaginary terms that can cause a mass flow error. Real terms are neglected. For a detailed derivation of the above equation we refer the reader to Rieder [15]. For the sake of physical clarity, we split the Young's Modulus into its real and imaginary parts $E_t + j E_{tw}$. In addition, the last term on the RHS shows up in the presence of an anti-symmetric component of the tube moment of inertia, I_{asym} . It is well known that such a component is inevitable in any real CMF system, owing to slight asymmetries in the tube clamping, which is different at the inlet and outlet sides. To demonstrate its effect we can assume the following simplified asymmetry factor multiplying the moment of inertia:

$$a_4(\zeta) = \begin{cases} -1, & \text{for } -1 \leq \zeta \leq -1 + \zeta_4 \\ 0, & \text{for } -1 + \zeta_4 \leq \zeta \leq 1 - \zeta_4 \\ +1, & \text{for } 1 - \zeta_4 \leq \zeta \leq 1 \end{cases} \quad (30)$$

where $\zeta_4 \ll 1$ is the dimensionless distance from the tube ends.

The perturbative contributions in Eq. (29) are formulated using the following auxiliary integrals:

$$\begin{aligned}
\Theta_{CC}^{sym,im} &= \int_{-1}^1 (\Phi_{IS}(\zeta) + \Psi_{IS}(\zeta)) a_C^2(\zeta) d\zeta \\
\Theta_{CC}^{sym,re} &= \int_{-1}^1 (\Phi_{RS}(\zeta) + \Psi_{RS}(\zeta)) a_C^2(\zeta) d\zeta \\
\tilde{C}_{DC} &= \int_{-1}^1 \left(1 - \alpha_0 \left(\frac{\rho_f - \rho_p}{\rho_f}\right)\right) a_D'(\zeta) a_C(\zeta) d\zeta \\
\Theta_{DC}^{sym} &= \int_{-1}^1 \left(\Phi_{RS}(\zeta) + \alpha_0 \left(\frac{\rho_f - \rho_p}{\rho_f}\right) + 2\Psi_{RS}(\zeta)\right) a_D'(\zeta) a_C(\zeta) d\zeta \\
\Theta_{DC}^{asym} &= \int_{-1}^1 (\Phi_{IA}(\zeta) + \Psi_{IA}(\zeta)) a_D(\zeta) a_C(\zeta) d\zeta \\
\Theta_{DC}^{asym,tube} &= \int_{-1}^1 a_D(\zeta) a_D'''(\zeta) a_C(\zeta) d\zeta
\end{aligned} \tag{31}$$

where we introduced the decomposition of the perturbation terms into symmetric (S) and anti-symmetric (A) as well as real (R) and imaginary (I) parts:

$$\begin{aligned}
\Phi(\zeta) &= \Phi_{RS}(\zeta) + \Phi_{RA}(\zeta) + j\Phi_{IS}(\zeta) + j\Phi_{IA}(\zeta) \\
\Psi(\zeta) &= \Psi_{RS}(\zeta) + \Psi_{RA}(\zeta) + j\Psi_{IS}(\zeta) + j\Psi_{IA}(\zeta).
\end{aligned} \tag{32}$$

It is important to note that all Θ integrals proportional to the different components of $\Psi(\zeta)$ and $\Phi(\zeta)$ are perturbations resulting from entrained particles, and are thus assumed small compared to all other terms, originating from the single-phase fluid equation. In addition, the perturbation to the clamping force proportional to $a_D(\zeta)$ is also small.

The physical meaning of the force terms for the LHS in Eq. (29), related to the Coriolis mode A_C is as follows:

- Modal stiffness force of tube (Real).
- Modal damping forces of tube, fluid and particles, proportional to energy loss (Imaginary). Damping forces are by factors smaller than the stiffness and inertial forces.
- Modal inertial forces of tube, fluid and particles, proportional to the densities (Real).

The meaning of the imaginary perturbation force terms at the RHS in Eq. (29), resulting from the driving mode A_D is as follows:

- Coriolis force with entrained particles, leading to the undisturbed apparent mass flow measurement (Imaginary).
- Coriolis force disturbance due to entrained particles, resulting in a relative mass flow error $E_m^{(1)}$ (Imaginary).
- Asymmetric damping term leading to the additional mass flow error in the presence of non-uniform particle distribution $E_m^{(2)}$ (Imaginary).
- Asymmetric damping term due to asymmetric components of the moment of inertia at the clamped tube ends, resulting in an absolute mass flow error $E_m^{(3)}$ (Imaginary).

Isolating the mass flow \dot{m} , and keeping only first order terms in the perturbation, we obtain the three corrections to the mass flow

$$\begin{aligned}
E_m^{(1)} &= \frac{\Theta_{DC}^{sym}}{\tilde{C}_{DC}} \\
E_m^{(2)} &= \left(\frac{l}{2}\right) \frac{\omega_D}{2v_f} \frac{\Theta_{DC}^{asym}}{\tilde{C}_{DC}} \\
E_m^{(3)} &= \left(\frac{2}{l}\right)^3 \frac{E_v J_{asym}}{(1-v^2)2\omega_D \dot{m}} \frac{\Theta_{DC}^{asym,tube}}{\tilde{C}_{DC}}
\end{aligned} \tag{33}$$

In the above derivation of $E_m^{(2)}$ we relied on the relation (10) and on the fact that $\dot{m} = \rho_f A_f v_f$. When deriving the error expressions, we also took into account that the damping forces are significantly smaller than the stiffness and inertia forces, and that the particles have the same effect on the natural frequencies of the driver mode and the Coriolis mode.

The relative mass flow measurement error $E_m^{(1)}$ is equivalent to the one derived previously due to entrained particles, including the symmetric compressibility and decoupling effects [3].

Table 1
Model parameters.

Symbol	Value	Description
l	0.4 m	tube axial length
d	0.026 m	tube inner diameter
d_o	0.03 m	tube outer diameter
ν	0.29	lateral-contraction number
E_t	$1.9 \cdot 10^{11}$ kg/m/s ²	tube Young-Modulus
ρ_t	$8.03 \cdot 10^3$ kg/m ³	tube material density
ρ_f	997 kg/m ³	fluid density
ρ_p	1.2 kg/m ³	particle density
c_f	1460 m/s	fluid speed of sound
c_p	340 m/s	particle speed of sound
γ	4/3	adiabatic gas constant
p	10^5 kg/m/s ²	fluid pressure
μ_f	10^{-3} kg/m/s	fluid dynamic viscosity
μ_p	10^{-5} kg/m/s	particle dynamic viscosity
a	3 or 95 μ m	particle radius (mp or fp)
v_f	1.1 m/s	fluid velocity
Q_r	10	resonator quality factor
f_D	200 Hz	driver frequency

The additional error $E_m^{(2)}$ is a new contribution to the error stemming from effects of non-uniform particle distribution along the tube axis. Such non-uniformity can lead to an anti-symmetric force component that is not accounted for by previous models. It is interesting to note that this error decreases with the flow velocity v_f .

The absolute error term $E_m^{(3)}$ is added to the mass flow in the presence of an anti-symmetric damping force at the clamped tube ends as described in Eq. (30). In Coriolis terminology, this offset is referred to as a zero-point error.

The diagram in Fig. 3 shows the physical factors that lead to the different mass flow errors. It is seen that in addition to the asymmetry of the moment of inertia $a_D(\zeta)$, the axial dependence of the particle radius $a(\zeta)$ and the particle volume fraction $\alpha(\zeta)$ are the error sources, where $\alpha(\zeta)$ is interchangeable with the term GVF for the present example with gas bubbles.

The particle radius and the particle volume fraction contribute to the phase decoupling effective area correction $\Phi(\zeta)$. The correction due to compressibility $\Psi(\zeta)$, however, is only affected by the change in sound velocity $c(\zeta)$ due to the axial dependent particle volume fraction $\alpha(\zeta)$. As seen above, the corrections Φ and Ψ directly contribute to the error terms $E_m^{(1)}$ and $E_m^{(2)}$. The mass flow error term $E_m^{(3)}$ is a consequence of an asymmetric damping force at the tubes ends.

3. Estimation of the magnitude of the mass flow error

To estimate the additional mass flow error we use the parameter values specified in Table 1. In addition we use the relations $A_f = \pi d^2$, $A_t = \pi(d_o^2 - d^2)$, and $I_t = \frac{\pi}{4}(d_o^4 - d^4)$.

To the particle radius a we assigned two different values, representing two physical limits, following the definition in Basse [3]. In the micro-particles (mp) limit, dominated by compressibility effects, the particle radius $a = 3 \mu$ m is much smaller than the characteristic viscous sub-layer thickness $\delta = \sqrt{2\mu_f/(\omega\rho_f)} \sim 40\mu$ m. The opposite limit of free particles (fp), where $a = 95\mu$ m $>$ δ , is dominated by the phase decoupling (bubble) effect.

The modal frequencies ω_D and ω_C can then be derived using Eq. (10) with the unperturbed Eigenvalues. The resulting driver frequency is then of the order of $f_D = \omega_D/(2\pi)$.

Two crucial inputs to the mass flow error model above are the ζ dependencies of the particle radius a and the particle volume fraction α . We adopt a simple model of these axial dependencies, based on the known fact that slight pressure differences between the inlet and the outlet sides of the tube always exist in the Coriolis measurement setup. For a more in deep analysis of the individual force loads and the corresponding errors, a statistical distribution function of these

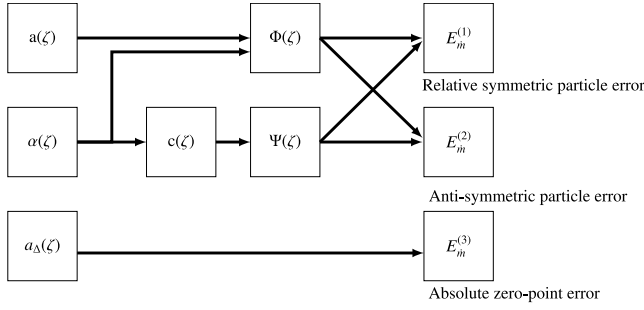


Fig. 3. Influence diagram of external factors on the mass flow error contributions. The axial dependence of the particle radius a and the particle fraction α lead to the force perturbations Ψ and Φ , which in turn cause the measurement errors $E_m^{(1)}$ and $E_m^{(2)}$. The asymmetry of the moment of inertia, a_Δ leads to an additional measurement error $E_m^{(3)}$.

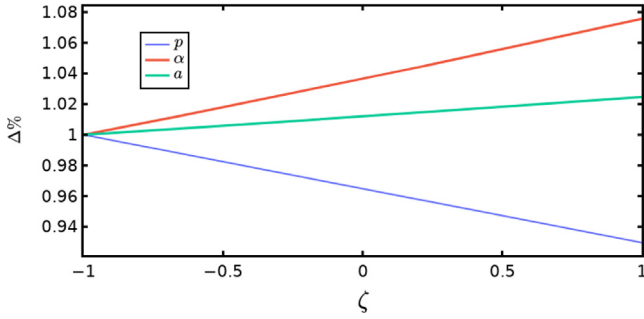


Fig. 4. Modeling the effects of pressure loss along the tube. The relative change in pressure p , particle fraction α , and particle radius a is shown as function of the axial coordinate ζ .

axial dependent variables can also be applied. The errors from each individual distribution can then be collectively combined. The magnitude of the pressure difference can be estimated based on previous publications [16] to be of the order of

$$\Delta p = \frac{2fG_m^2 l}{\rho_m d}. \quad (34)$$

Where f is the Darcy friction factor, mass flux G_m and the mixture density ρ_m according to Awad and Muzychka [17]. A simple model of the resulting pressure drop along the tube assumes a linear behavior. As a consequence, we expect the mean particle volume to increase linearly along the tube such that the product $p_i V_i$ remains constant for a given fluid cell i along the tube. This in turn leads to an increase in the mean particle radius which is proportional to the third root of the volume drop. The axial dependencies assumed in this simplified model are sketched in Fig. 4. For the sake of simplicity we neglect additional spatial dependencies of a and α , even though they generally exist.

As already mentioned, the pressure loss is only one potential source of asymmetric influences. Other influences can be caused by the geometry of the measuring tube and the introduction of particles into the fluid itself. The asymmetry generated does not have to follow a linear progression.

The axial dependencies of a and α lead to an axial dependence of the perturbation terms $\Psi(\zeta)$ and $\Phi(\zeta)$. In Fig. 5 we show the ζ dependencies of Ψ and Φ , split into their different components, calculated assuming the linear pressure drop depicted in Fig. 4. We note that since the anti-symmetric corrections are around two orders of magnitude smaller than the symmetric ones, we use separate y-axes for the symmetric (left axis) and anti-symmetric (right axis) perturbation terms. The different panels of Fig. 5 show the effect of all corrections for three different values of the particle fraction α , in the limit of free particles (left column) as well as for micro particles (right column). As expected, all of the effects grow with α , thereby leading to larger measurement errors of the mass flow.

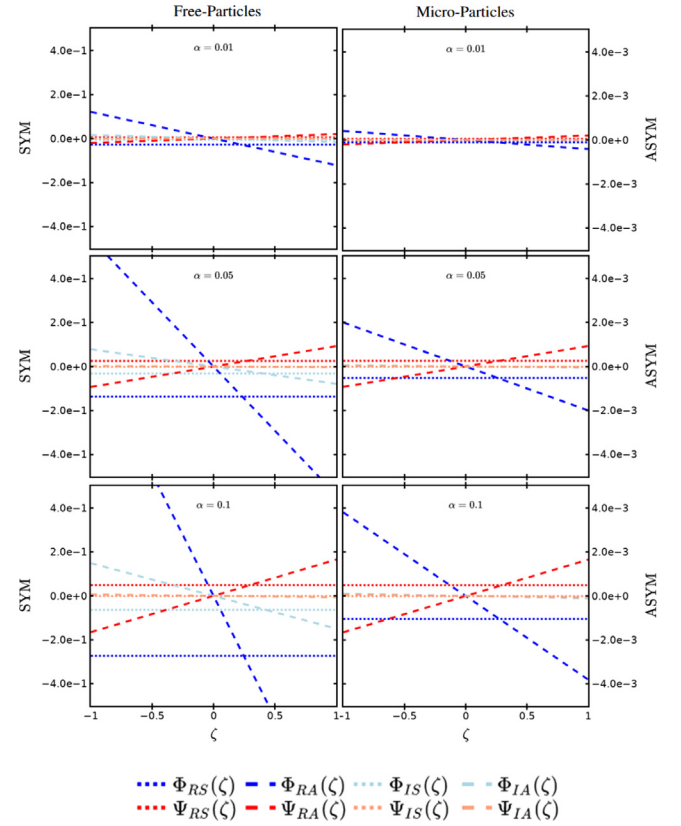


Fig. 5. Quantifying the axial dependence of the effective force perturbations. The real (R) and imaginary (I) symmetric (S) and anti-symmetric (A) components of the perturbation terms $\Psi(\zeta)$ and $\Phi(\zeta)$ are plotted against the axial coordinate ζ in the free particles (left column) and micro-particles (right column) limits, for 3 different particle fractions $\alpha = 0.01, 0.05, 0.1$ (top to bottom panels). Refer to the left-hand (right-hand) y axis for symmetric (anti-symmetric) corrections.

The resulting mass flow errors can be observed directly in Fig. 6 in the two regimes of free particles (red) and micro particles (blue). In each regime we plot three curves: $E_m^{(1)}$ is the previously known error due to uniform entrained particles (dotted lines). $E_m^{(1+2)} = E_m^{(1)} + E_m^{(2)}$ is the combined error when non uniformity of the particles is considered (solid lines). Note that here we neglected the correction $E_m^{(3)}$ in order to keep the model assumptions simple. The third curve (gray) corresponds to the error E_m^B ,

$$E_m^B = \frac{\alpha(\rho_F - \rho_P)(1 - F)}{\alpha\rho_P + (1 - \alpha)\rho_F} + \frac{1}{2} \left(\frac{\omega}{c} d/2 \right)^2 \quad (35)$$

as calculated in Basse [3], for the sake of comparison of our derivation of $E_m^{(1)}$ with previous models. Indeed, there is a good agreement between the previously calculated error and our calculation.

As can be seen in Fig. 6, the anti-symmetric effect of a non uniform particle distribution along the tube is small in the limit of micro particles but significant in the limit of free particles. It amounts to a positive correction, thereby partially compensating the symmetric error contribution due to uniform entrained particles.

4. Conclusion

In this paper we calculated corrections to the mass flow measurement in a Coriolis measurement device. We introduced a way to add perturbations into the equation of motion, which allowed us to model the presence of entrained particles in the measured fluid. In contrast to previous models of the mass flow errors, our model goes beyond the common assumption of uniform distribution of entrained particles, and allows for variations in the particle radius and concentration. We

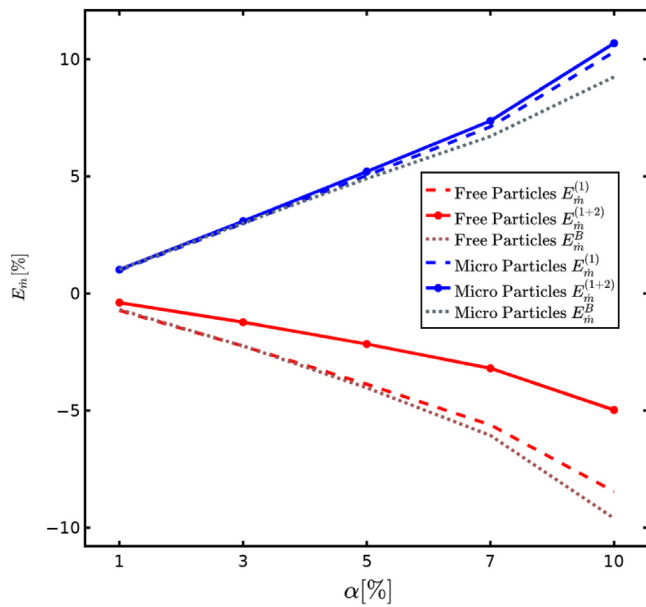


Fig. 6. Analytically calculated mass flow errors. The relative mass flow error in the presence of non-uniform entrained particles $E_m^{(1+2)}$ is plotted against the particle fraction α in the free particles (solid red) and the micro-particles (solid blue) limits. It is compared with the respective errors $E_m^{(1)}$ assuming uniform entrained particle distribution in the two limits (dashed lines), and with previously calculated errors $E_m^{(B)}$ (dotted lines).

showed that this non uniformity leads to an additional measurement error on top of the previously calculated one. We estimated the magnitude of the new error, and showed that it is particularly significant in the limit of free entrained particles, and thus should not be neglected in realistic measurement conditions. Our future research is focused on an experimental verification of the measurement errors that are derived here.

Nomenclature

Indexes, Prefixes, Over and Underlining	
•:	Placeholder for indexes and prefixes
Δ	Difference
A	Anti-symmetric component
$asym$	Anti-symmetric component
C	Coriolis mode
$comp$	Compressibility
D	Driver mode
dec	Decoupling
f	Fluid
I	Imaginary component
m	Mixture
p	Particle
R	Real component
r	Resonator
S	Symmetric component
sym	Symmetric component
t	Tube
Latin Symbols	
\dot{m}	Mass flow
a	Radius particle
A_c	Cross-sectional area, Modal amplitude
$a_n(\zeta)$	Eigenform

$a_\Delta(\zeta)$	Anti-symmetric evaluation function
c	Speed of sound
d	Tube inner diameter
d_o	Tube outer diameter
E_s	Young-Modulus
F	Force factor
f	Darcy friction factor
f_s	Frequency
G_m	Mass flux
I_s	Moment of inertia
k_s	Yieldingness
l	Tube axial length
p	Pressure
Q_r	Resonator quality factor
t	Time
v_s	Velocity
x	Coordinate of Cartesian system
z	Coordinate of Cartesian system
Greek Symbols	
δ	Characteristic viscous sub-layer thickness
γ	Adiabatic gas constant
γ_s	Eigenvalues
ν	Lateral-contraction number
ω_s	Angular frequency
Φ_s	Bubble effect
Ψ_s	Resonator effect
Θ_s	Auxiliary integrals
ζ	Dimensionless axial coordinate
α	Gas void fraction (GVF)
μ_s	Dynamic viscosity
ρ_s	Density
Other Symbols	
π	Circular number
j	Complex symbol

CRedit authorship contribution statement

Stephan Wernli: Writing – original draft, Visualization, Software, Project administration, Investigation, Formal analysis. **Lilach Goren Huber:** Writing – review & editing, Validation, Supervision, Investigation, Formal analysis. **Nicolas P. Avdelidis:** Writing – review & editing, Validation. **Alfred Rieder:** Writing – review & editing, Writing – original draft, Supervision, Resources, Investigation, Formal analysis.

Declaration of competing interest

The authors declare the following financial interests/personal relationships which may be considered as potential competing interests: Stephan Wernli reports financial support was provided by Endress Hauser Flowtec AG. Stephan Wernli reports a relationship with Endress Hauser Flowtec AG that includes: employment and funding grants. If there are other authors, they declare that they have no known competing financial interests or personal relationships that could have appeared to influence the work reported in this paper.

Alfred Rieder reports financial support was provided by Endress Hauser Flow Deutschland AG. Alfred Rieder reports a relationship with Endress Hauser Flow Deutschland AG that includes: employment. If there are other authors, they declare that they have no known competing financial interests or personal relationships that could have appeared to influence the work reported in this paper.

Acknowledgments

The authors would like to express their gratitude to Endress + Hauser Flow for supporting the study. The authors would also thank Dr. Yaoying Lin and Dr. Andreas Güttler for valuable discussions and inputs.

Data availability

No data was used for the research described in the article.

References

- [1] T. Wang, R. Baker, Coriolis flowmeters: a review of developments over the past 20 years, and an assessment of the state of the art and likely future directions, *Flow Meas. Instrum.* 40 (2014) 99–123, <http://dx.doi.org/10.1016/j.flowmeasinst.2014.08.015>.
- [2] M. Anklin, W. Drahm, A. Rieder, Coriolis mass flowmeters: Overview of the current state of the art and latest research, *Flow Meas. Instrum.* 17 (6) (2006) 317–323, <http://dx.doi.org/10.1016/j.flowmeasinst.2006.07.004>, URL <https://www.sciencedirect.com/science/article/pii/S0955598606000379>, Coriolis Massflow Meters.
- [3] N.T. Basse, A review of the theory of Coriolis flowmeter measurement errors due to entrained particles, *Flow Meas. Instrum.* 37 (2014) 107–118, <http://dx.doi.org/10.1016/j.flowmeasinst.2014.03.009>, URL <https://www.sciencedirect.com/science/article/pii/S095559861400034X>.
- [4] A. Rieder, H. Zhu, Coriolis mass flowmeters: On measurement errors in two-phase conditions, in: *Proceedings of the 13th International Flow Measurement Conference (FLOMEKO 2005)*, International Measurement Confederation (IMEKO), Peebles, Scotland, United Kingdom, 2005.
- [5] J. Weinstein, *The motion of bubbles and particles in oscillating liquids with applications to multiphase flow in Coriolis meters*, 2008.
- [6] O.L. Ibryaeva, V.V. Barabanov, M.P. Henry, M. Tombs, F. Zhou, A benchmark data set for two-phase Coriolis metering, *Flow Meas. Instrum.* 72 (2020) <http://dx.doi.org/10.1016/j.flowmeasinst.2020.101721>.
- [7] J. Hemp, J. Kutin, Theory of errors in coriolis flowmeter readings due to compressibility of the fluid being metered, *Flow Meas. Instrum.* 17 (6) (2006) 359–369, <http://dx.doi.org/10.1016/j.flowmeasinst.2006.07.006>, URL <https://www.sciencedirect.com/science/article/pii/S095559860600046X>, Coriolis Massflow Meters.
- [8] A. Rieder, W. Drahm, H. Zhu, *In-line measuring devices and method for compensation of measurement errors in in-line measuring devices*, 2008, United States Patent, Patent No. US7360453B2.
- [9] M. Henry, M. Tombs, M. Zamora, F. Zhou, Coriolis mass flow metering for three-phase flow: A case study, *Flow Meas. Instrum.* 30 (2013) 112–122, <http://dx.doi.org/10.1016/j.flowmeasinst.2013.01.003>, URL <https://www.sciencedirect.com/science/article/pii/S0955598613000095>.
- [10] D.L. Gysling, Accurate mass flow and density of bubbly liquids using speed of sound augmented Coriolis technology, *Flow Meas. Instrum.* 91 (2023) 102358, <http://dx.doi.org/10.1016/j.flowmeasinst.2023.102358>, URL <https://www.sciencedirect.com/science/article/pii/S0955598623000547>.
- [11] Endress+Hauser Flow, Proline, Promass I: Coriolis mass flow measurement, 2016, Field instrument, Business Area: Flow. Product Family: Promass I. Graphics View: Cut away drawing.
- [12] W. Young, R. Budynas, *Roark's formulas for stress and strain*, in: MacGraw-Hill international edition, McGraw Hill LLC, 2001, URL <https://books.google.ch/books?id=pummCLoFXEC>.
- [13] R. Singiresu, V.T.T. Nguyen, *Mechanical Vibrations*, fifth ed., Pearson, Upper Saddle River, NJ, 2011, pp. 721–726.
- [14] N.T. Basse, Coriolis flowmeter damping for two-phase flow due to decoupling, *Flow Meas. Instrum.* 52 (2016) 40–52, <http://dx.doi.org/10.1016/j.flowmeasinst.2016.09.005>, URL <https://www.sciencedirect.com/science/article/pii/S0955598616301510>.
- [15] A. Rieder, *Modellgestützte Auslegung und Realisierung eines Coriolis-massedurchflussmessers mit einem geraden Meßrohr*, Als Ms. gedr., in: *Fortschritt-Berichte VDI*, VDI-Verl., Düsseldorf, 1998, Literaturverz. S. 114 - 118.
- [16] S.M. Bhagwat, A.J. Ghajar, A flow pattern independent drift flux model based void fraction correlation for a wide range of gas-liquid two phase flow, *Int. J. Multiph. Flow* 59 (2014) 186–205, <http://dx.doi.org/10.1016/j.ijmultiphaseflow.2013.11.001>, URL <https://www.sciencedirect.com/science/article/pii/S0301932213001705>.
- [17] M. Awad, Y. Muzychka, A robust asymptotically based modeling approach for two-phase flows, *Adv. Mech. Eng.* 2014 (2015) <http://dx.doi.org/10.1155/2014/327653>.

Coriolis massflow measurement errors due to inhomogeneous entrained particles: an analytical model

Wernli, Stephan

2025-06

Attribution-NonCommercial 4.0 International

Wernli S, Huber LG, Avdelidis NP, Rieder A. (2025) Coriolis massflow measurement errors due to inhomogeneous entrained particles: An analytical model. *Flow Measurement and Instrumentation*, Volume 103, June 2025, Article number 102847

<https://doi.org/10.1016/j.flowmeasinst.2025.102847>

Downloaded from CERES Research Repository, Cranfield University